Title

High-Performance, Wearable Thermoelectric Generator Based on a Highly Aligned Carbon Nanotube Sheet

Journal

ACS Applied Energy Materials, 3(1)

ISSN

2574-0962

Authors

Choi, Jaeyoo
Jung, Yeonsu
Dun, Chaochao
et al.

Publication Date

2020-01-27

DOI

10.1021/acsaem.9b02255

Peer reviewed

High-Performance, Wearable Thermoelectric Generator based on Highly-Aligned Carbon Nanotube Sheet

Jaeyoo Choi [1,2,3,+], Yeonsu Jung [2,4,+], Chaochao Dun [1], Kyung Tae Park [2,3], Madeleine P. Gordon [1,5], Kyle Haas [1,6], Pengyu Yuan [1,7,8], Heesuk Kim [3,9,*], Chong Rae Park [2,*], Jeffrey J. Urban [1,*]

[1] The Molecular Foundry Lawrence Berkeley National Laboratory Berkeley, CA 94720,

[2] Carbon Nanomaterials Design Laboratory, Research Institute of Advanced Materials, Department of Materials Science and Engineering, Seoul National University, Seoul, 08826, Republic of Korea

[3] Photo-electronic Hybrids Research Center, Korea Institute of Science and Technology (KIST), Seoul, 02792, Republic of Korea

[4] Composites Research Division, Korea Institute of Materials Science, Changwon, 51508, Republic of Korea

[5] Applied Science and Technology Graduate Group, University of California, Berkeley, California, 94720, USA

[6] College of Engineering, University of California, Berkeley, California, 94720, USA

[7] Department of Mechanical Engineering, University of California, Berkeley, California, 94720, USA

[8] School of Engineering, University of California, Merced, California, 95343, USA

[9] Nano-Materials and Engineering, Korea University of Science and Technology (UST), Daejeon, 34113, Republic of Korea

Corresponding authors: heesukkim@kist.re.kr; crpark@snu.ac.kr; jjurban@lbl.gov

[+] These authors equally contributed to this work.

Abstract

In this paper, a high-performance, wearable thermoelectric generator (TEG) was fabricated with a highly-aligned carbon nanotube (CNT) sheet. The aligned CNT sheet exhibits extraordinary electrical conductivity compared to disordered CNT sheets and also can be directly fabricated as a continuous TEG without metal electrode interconnects. This provides a significant reduction in contact resistance between TE legs and electrodes compared to traditional TEGs, resulting in higher power output. In addition, the continuity of the module without any disconnected parts provides high degrees of mechanical stability and durability. This robust and scalable approach to flexible TEG fabrication paves the way for CNT applications in lightweight, flexible, and wearable electronics.

Keywords: Carbon nanotube sheet, highly-aligned structure, thermoelectric energy conversion, flexible thermoelectric generator, wearable device.

Introduction

Soft thermoelectric (TE) materials can be used for the fabrication of flexible energy converters with conformal geometries and are highly promising materials currently enabling a new portfolio of TE applications.[1] Among them, carbon nanotube (CNTs) based TE devices have attracted considerable attention because of its potential for high electrical conductivity,[2-3] as well as its ability to fully recover from severe bending or compression.[4] Additionally, the carrier concentration and carrier types of CNTs are easily controlled by chemical doping[5] providing a great platform to utilize them as electrical legs for flexible/wearable TE applications. Yet while researchers have been able to report promising papers on CNT composite films,[6-9] doping and fabrication techniques,[10-14] and TE applications,[6] their commercial viability as flexible TE devices is lacking due to insufficient performance.

For example, the typical power output of flexible CNT-based TE devices (μW scale) is still several orders of magnitude lower than their bulk inorganic counterparts (mW scale) such as Bi_2Te_3-Sb_2Te_3.[6, 15-18] Fundamentally, a number of factors must be overcome to achieve higher performances. The poor TE properties observed in CNTs derive from the metallic conduction behavior of CNTs in bulk even though the bulk mixture is typically comprised of both semiconducting and metallic CNTs.[19] As a result, the Seebeck coefficient (S) of typical CNTs has so far been limited to 70 μV/K.[6] Many researchers are currently attempting to solve this issue by separating

semiconducting and metallic nanotubes.[20-22] Another obstacle is that the as-reported CNT systems necessarily require additional electrode deposition, where typical metal electrodes such as Cu and Ag form poor physical contacts and energetic mismatches with CNTs, resulting in non-ohmic contacts.[18, 23-24] Therefore, the circuit resistance of the as-reported TE generators (TEGs) based on CNTs is much higher than theoretical expectations despite the very low resistance of the CNTs themselves. These factors compounded together translates into overall poor TE performance of CNT modules. Further complicating their use as electronic devices, the electromechanical properties of CNTs are prone to deterioration over time from decreased adherence between the electrodes and functional legs.[25] Resultingly, low performance and the lack of mechanical durability between contacts remain a significant barrier for commercial viability and widespread deployment.

To address these issues, we have previously proposed a continuously fabricated pure CNT yarn TEG with high performance and robustness.[26] This flexible TEG (*f*-TEG) was innovative in that the long, single-thread CNT yarn can be multi functionalized with *p*- and *n*-type legs and electrodes without requiring additional deposition processes. This continuous module structure is beneficial in minimizing the circuit resistance of the module, enabling both high performance and mechanical stability. In this paper, we build upon those initial results and take the next steps to design, fabricate, and optimize a wearable *f*-TEG based on a highly-aligned CNT sheet directly synthesized

by floating catalyst chemical vapor deposition (FCCVD).[27] Due to the highly-aligned structure of the CNT web, the present CNT sheet exhibits superior TE properties in comparison to the disordered CNT sheet. A facile solution-based chemical doping technique was used to make both *p*- and *n*-type CNT sheets and to create the continuous CNT module without additional metal electrodes. This innovative continuous module design is beneficial when applied as a *f*-TEG because of improved electromechanical stability and durability, two crucial requirements for real-world application.

For a systematic study of minimizing the overall circuit resistance and maximizing their TE performance, we fabricated 3 different structures of TE modules with various CNT sheets and compared their TE performances. Additionally, we fabricated a wristband-prototype *f*-TEG and yield a maximum output power of 8 μW when exposed to a 50 K temperature gradient. We also demonstrated that this prototype *f*-TEG enables effective electrical generation from body heat. In conclusion, due to our highly-aligned CNT sheet's extraordinary electromechanical properties and its low density (~0.4 g/cm^3) compared to that of bulk inorganic Bi_2Te_3 (~7.86 g/cm^3),[26] the present *f*-TEG possesses enormous potentials for wearable TE applications.

Experimental Section

Synthesis of CNT sheet. CNTs were synthesized by a floating catalyst method as previously reported.[26-27] Ferrocene, thiophene, and methane were

used as a catalyst precursor, promoter, and carbon source for CNT synthesis at 1200 °C, respectively. CNTs are highly integrated into aerogel-like forms in a reactor. These aerogel forms can be continuously withdrawn from the reactor at the bottom. The CNT sheet was prepared such that an aerogel was directly wound on a cylindrical roller. All chemical reagents were purchased from Sigma-Aldrich and used as received.

Fabrication of flexible TEG. To fabricate the traditional design modules in **Figure 2a**, 5 mg of commercial Single-walled CNTs (SWCNT, TNST grade, Chengdu Organic Chemicals Co., Ltd) were added in 100 ml of Ethanol (Sigma-Aldrich) and dispersed well via tip sonication for 30 min. The commercial SWCNT films were then prepared by vacuum-filtering the mixed suspensions through cellulose membrane filters (Milipore) with a 45-mm diameter and 0.2 μm average pore size. For the fabrication of traditional module in **Figure 2a** and 2**b**, the vacuum filtered commercial SWCNT sheet and as-synthesized CNT sheet were cut in the proper size (2 × 1 cm^2). Then 5 of the CNT sheets were *p*-doped with a $FeCl_3$ ethanol solution (Sigma-Aldrich, 2mM) for 30 min and another 5 CNT sheets were *n*-doped with a polyethyleneimine ethanol solution (PEI (MW = 600 g/mol), Sigma-Aldrich, 8 mM) for 30 min, followed by drying in ambient conditions. 5 pairs of p- and n-doped CNT sheets were alternately connected in series by using silver paste (Sigma-Aldrich). Scotch tapes (3M) were used as insulating layers. To fabricate the continuous module in **Figure 2c**, the as-synthesized CNT sheet was cut in the proper size (20 × 1 cm^2) and *p*, *n*-doped with the same

dopants as detailed above. For accurate doping, 2 × 1 cm^2 glass slides were used to cover the un-doped area. The narrow un-doped regions between *p*, *n*-doped areas are used as electrodes. After drying well, the CNT sheet was folded at the un-doped regions and scotch tape was used as insulating layers between the folded legs.

Fabrication of the prototype TEG. The as-synthesized CNT sheet was cut to a size of 20 × 1.5 cm^2 and alternatively *p*, *n*-doped with the same dopants and methods as detailed in the above section. We controlled the size of the doped area for 1 cm and un-doped areas for 2 mm long. After drying well in ambient conditions, the doped CNT sheet was woven into the as-prepared Polydimethylsiloxane (PDMS, Sylgard 184) flexible support unit. The PDMS unit was prepared by using the homemade stainless steel mold in **Figure S5**. The 9 pairs of *p*, *n*-doped CNT sheets were fabricated as a prototype TEG.

Characterization. The microstructural morphology of the synthesized CNT sheet was investigated using high-resolution TEM (HR-TEM, JEOL, JEM-2100F) and field-emission SEM (FE-SEM, ZEISS, MERLIN Compact). The polarized Raman spectroscopy (RAMANplus, Nanophoton) with a 532 nm laser and 2D Wide-Angle X-ray Scattering (WAXS, Bruker, D8 Discover) were used to quantify the CNT alignment. The intensities of the *G*-band were recorded when the incident laser beam was placed parallel and perpendicular to the longitude direction of the CNT sheet, and their ratio was used to describe the alignment of CNTs. The TE properties of the as-prepared samples deposited

on glass substrates with a dimension of 2×1 cm^2 were analyzed by measuring electrical conductivity (σ) and Seebeck coefficient (S) at room temperature. The in-plane resistance (R) and S of the samples were simultaneously measured using a four-point probe TE measurement system (TEP 600, Seepel instrument), and the average values of at least 10 measurements were taken. For Seebeck coefficient measurement, the potential differences arising from temperature differences between the two ends of the sample (0.5, 1.5, and 2.5 °C at one end, and -0.5, -1.5, and -2.5 °C at the other) were recorded and the corresponding *S* was calculated based on the slope. These values were considered to be reliable when the linear correlation (R^2) of the measured potential differences was higher than 0.999. The carrier concentration and mobility were determined by Hall measurements (HMS-5000, Ecopia) with a 0.55 T and 1 mA, with an average value of at least 10 measurements. The circuit resistance and open circuit voltage of module were measured by Keithley 2700 acquirement system. Two ends of a module were connected in series with the measurement system. The output power of the module was measured using a homemade system: by applying a current to a pair of Peltier modules, the bottom side is cooled and the top side is heated. The temperature at each side is automatically controlled by a temperature controller unit (Wavelength electronics, LFI-3751). Metal heat sinks are equipped to maintain a stable temperature gradient. For the demonstration of energy harvesting from body heat, the digital multimeter (Extech instrument) was used to measure the

circuit resistance and Seebeck voltage of the module. The thermal radiometric camera (OMEGA, FLIR E30) was used to record the thermal image.

Results and Discussion

Synthesis of highly-aligned CNT sheet

Floating catalyst chemical vapor deposition (FCCVD) used in this work has a great potential for production of large-area CNT sheet with excellent electrical and mechanical properties. **Figure 1a** shows the schematic illustration of the synthesis process for the highly-aligned CNT sheet. The aerogel like CNT assembly is formed in a hot reactor and it is possible to wind them up onto a roller continuously at the bottom of the reactor with stable feeding of the catalyst precursor and carbon source into the reactor. The macroscopic assembly of synthesized CNTs was consisted of multi-walled CNTs, having 5-7 walls with an outer diameter of about 15 nm, as shown in **Figure 1b**. The as-synthesized CNTs contain small amounts of iron catalyst of 7.6 wt%, as can be seen by the change in mass from thermogravimetric analysis (TGA) shown in **Figure S1**. There is a high degree of alignment in the winding direction of CNT web, which is described in **Figure 1c** and **1d,** corresponding to heightened electrical properties. To further study the aligned morphological structure, 2D WAXS measurement was performed. In **Figure 1e** and **1f**, increased scattering intensity can be

observed at certain points along the scattering ring. This higher degree of intensity is indicative of preferential alignment corresponding to that specific direction. This directionality is further confirmed through inspection of the azimuthal integration of (002) showing two distinct peaks. This clearly demonstrates that the CNT sheet is highly aligned in the winding direction of CNT web. The polarized Raman spectra in **Figure S2** provides further evidence of the highly-aligned nature of the as-prepared CNT sheet. The polarized Raman intensity factor[28] ($IG_{\parallel}/IG_{\perp}$, the ratio of *G* peak intensity parallel to the Raman laser to one in the vertical direction) of the as-synthesized CNT sheet is 1.48, stating that the CNT sheet is quite aligned compared to a ratio value of 1 for disordered CNT sheet. As a result, the CNT sheet synthesized by FCCVD has a high degree of alignment in the winding direction of CNT web.

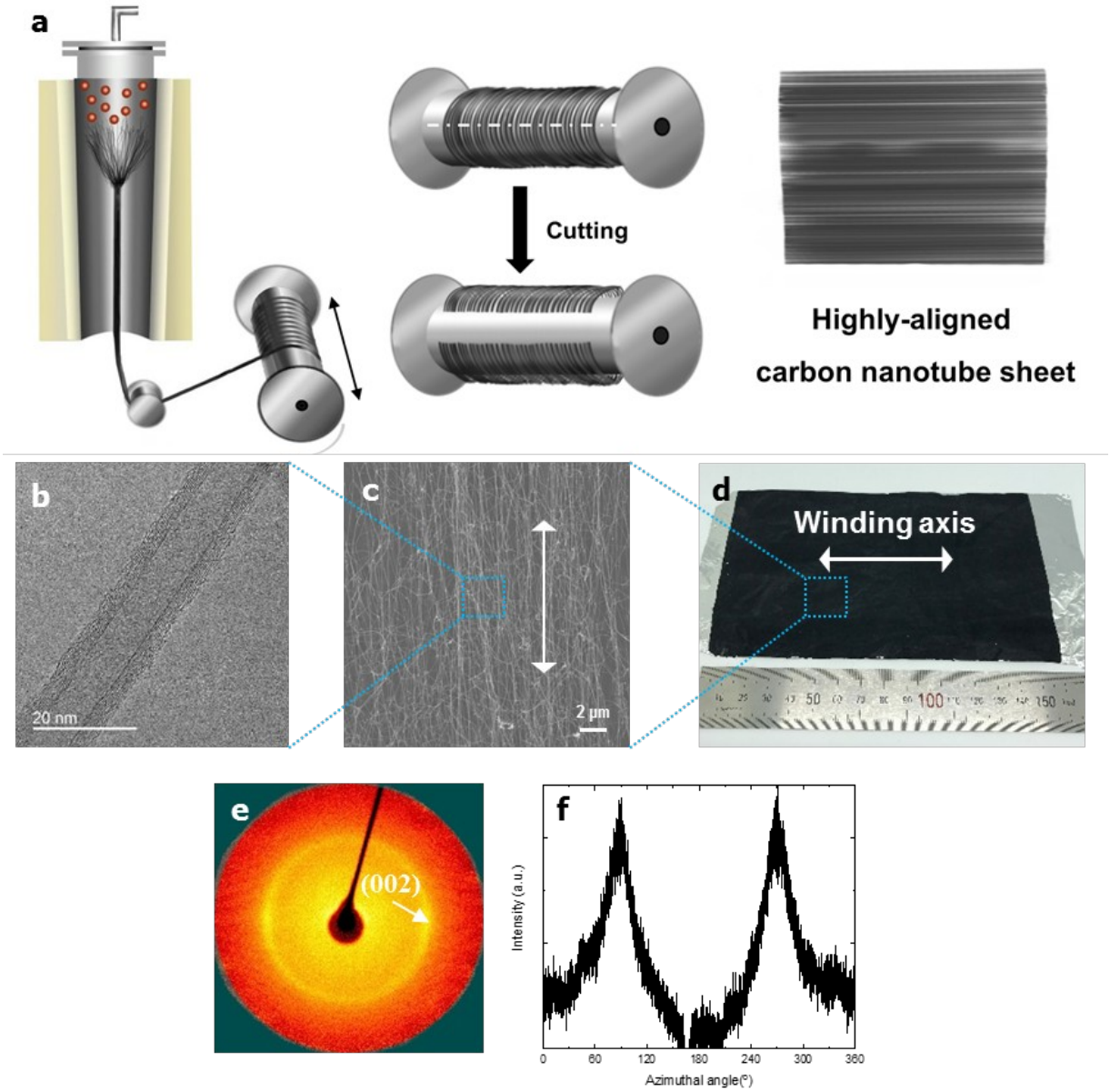

Figure 1. (a) Schematic image of the preparation process of highly-aligned CNT sheet by FCCVD (b) HR-TEM and (c) FE-SEM images of the as-synthesized CNT and aerogel-like assembly. (d) Photo image of large area CNT sheet (white arrows in c and d indicate the winding axis) (e) 2D WAXS pattern and (f) azimuthal angle scan profile of (002) for CNT sheet.

Thermoelectric properties of highly-aligned CNT sheet

The performance of TE materials is evaluated by a dimensionless figure-of-merit (ZT), which is defined as $ZT=S^2\sigma T/\kappa$, where S is the Seebeck coefficient, σ is the electrical conductivity, and κ is the thermal conductivity, respectively. For our system, we will discuss an increase in power factor (PF, $S^2\sigma$) rather than enhancement in ZT, due to difficulty in thermal conductivity measurement of CNT thin film. **Table 1** lists the TE properties including σ, S, PF, carrier concentration (n), and carrier mobility (μ) of various vacuum filtered CNT sheets prepared by commercial MWCNTs and SWCNTs, as well as the present highly-aligned CNT sheet.

Table 1. Thermoelectric properties of various CNT sheets at room temperature.

Transport parameters	Thickness (μm)	Electrical conductivity (S/m)	Seebeck coefficient (μV/K)	Power factor (μW/m·K^2)	Carrier concentration (10^{22}/cm^3)	Carrier mobility (cm^2/v·s)
Vacuum filtered MWCNT sheet (Disordered structure)	30	1300	8	0.1	0.05	0.08
Vacuum filtered SWCNT sheet (Disordered structure)	30	34400	42	61	1.14	0.48
FCCVD CNT sheet, in this work (Highly-aligned structure)	20	50600	56	158	1.01	0.88

It is seen that the disordered vacuum filtered MWCNT sheet has a relatively low σ of 1.3 $\times 10^3$ S/m compared to the SWCNT sheet due to its low n $\sim 5.0 \times 10^{20}$ cm^{-3} and $\mu \sim 0.08$ $cm^2/v \bullet s$. On the contrary, it should be noted that the highly-aligned CNT sheet synthesized by FCCVD shows a higher σ of 5.06 $\times 10^4$ S/m despite being composed of few-walled CNTs similar to MWCNT. From the measured n and μ of the SWCNT sheet and the as-synthesized CNT sheet, it is apparent that the increased σ of the as-synthesized CNT sheet is predominantly due to the increase of μ. We attribute this notable increase of μ to the better interconnections between CNTs as a result of the highly-aligned structure. In addition, the as-synthesized CNTs by FCCVD have been shown in literature not only to have a high aspect ratio but also to contain fewer defects and impurities, such as amorphous carbon.[27] These are well-matched with the results that the μ of the highly-aligned CNT sheet (~ 0.88 $cm^2/v \bullet s$) is 11 times higher than that of the vacuum filtered MWCNT sheet, and 1.8 times higher than that of the vacuum filtered SWCNT sheet. Here, the highly-aligned CNT sheet shows a higher S than the vacuum filtered SWCNT sheet with the decreased n, which generally follows the trend of Mott's relationship.[29] However, both vacuum filtered SWCNT and FCCVD CNT sheets show an increased n and a higher S compared with the vacuum filtered MWCNT sheet. This phenomenon might be related to the different density of state (DOS) and Fermi level between SWCNT and MWCNT, but further exploration would need to be done to detangle these complex effects.

TEGs usually consist of *p*- and *n*-type legs electronically connected in series and thermally connected in parallel to achieve maximum device efficiency. However, it is generally accepted that pristine CNT shows *p*-type behavior because oxygen and moisture are naturally doped from the air.[30] Therefore, chemical doping is required to either improve the *p*-type TE properties of CNTs or achieve *n*-type CNTs. To optimize the TE properties of our CNT sheet, *p*- and *n*-type doping were achieved by a simple solution process with suitable chemical dopants. Polyethylenimine (PEI) is a common yet effective *n*-type dopant that can drastically change the property of CNT from *p*-type to *n*-type.[5] This is because physical adsorption of PEI on the CNT wall enables the amine groups in the PEI to donate electrons to the CNT resulting in a switch from p-type to n-type characteristic.[31-32] For a *p*-type dopant, we chose $FeCl_3$, which induces a redox reaction between CNTs and $FeCl_3$ causing the Fe^{3+} ions to reduce to Fe.[33-34] During the reduction process, electrons are extracted from the CNTs resulting in strong *p*-type doping. The chemical structures of the *p*- and *n*-type dopants used in this study are illustrated in **Figure S3**. **Table 2** lists the TE properties of *p*- and *n*-doped CNT sheets. Both chemically doped CNT sheets show a dramatic enhancement in σ with little to no decrease of *S*, which is ideal for preparing functional *f*-TEGs with lower internal resistance.

Table 2. Thermoelectric properties of *p*, *n*-doped CNT sheet at room temperature.

Transport parameters	***p*-doped**	***n*-doped**

	CNT sheet	CNT sheet
Thickness (μm)	20	20
Electrical conductivity (S/m)	81300	79000
Seebeck Coefficient (μV/K)	55	-57
Power factor (μW/m•K^2)	250	255
Carrier concentration (10^{22}/cm^3)	2.08	1.08
Carrier Mobility (cm^2/v•s)	0.62	0.81

After *p*-type doping, the *n* increases while the μ decreases slightly due to enhanced carrier scattering. By *n*-type doping, the CNT sheet successfully demonstrated *n*-type behavior but showed no major change in *n* and μ. Temperature-dependent TE measurements of *p*- and *n*-doped CNT sheets were also performed in the range of 300-550 K and are shown in **Figure S4**. The σ of both CNT sheets decreases with an increase of temperature, indicating the metallic behavior of the CNT sheet. Additionally, the *n*-doped CNT sheet shows a conversion from *n*- to *p*-type around 480 K, which is likely due to the dissociation of PEI dopant at high temperature. After doping, *p*- and *n*-doped CNT sheets show a PF of 250 and 255 μW/m•K^2, respectively.

Continuous module design for minimizing circuit resistance

Traditional TE modules are generally arranged in a way that the temperature gradient is formed along the in-plane direction of each leg. However, more modules are being designed so that a temperature gradient is formed along

the cross-plane direction of each leg as it allows TE modules to be used in diverse applications. Traditional materials with high rigidity and anisotropy have restrictions to fabricate both module design, and the TE performance in the cross-plane direction is less competitive than the in-plane ones in some cases. Thanks to the flexibility and mechanical stability of the CNT sheet, our system allows for a great degree of freedom when designing module type and structure. Highly-conductive CNT sheets can not only act as the module legs with proper doping but when undoped it could act as the connecting electrode as well, thus enabling innovative module design such as a continuous module electrically connected in series without metal electrodes. This creative design could provide not only mechanical flexibility and durability but also TE performance enhancement through minimizing circuit resistance. For the systematic study of this, we prepared three different types of flexible TE modules with 5 pairs of alternating *p*- and *n*-doped CNT sheets. **Figure 2a, b, and c** show the schematic images of them. The first module in 2a (module A) is the typical module design with stacked CNT sheets prepared by vacuum filtration of commercial SWCNT dispersed solution. Each doped CNT sheet was electrically connected in series by metal electrodes (Ag paste). With the results in **Figure S2**, we concluded that the vacuum filtered CNT sheet has a disordered structure with a low degree of alignment.

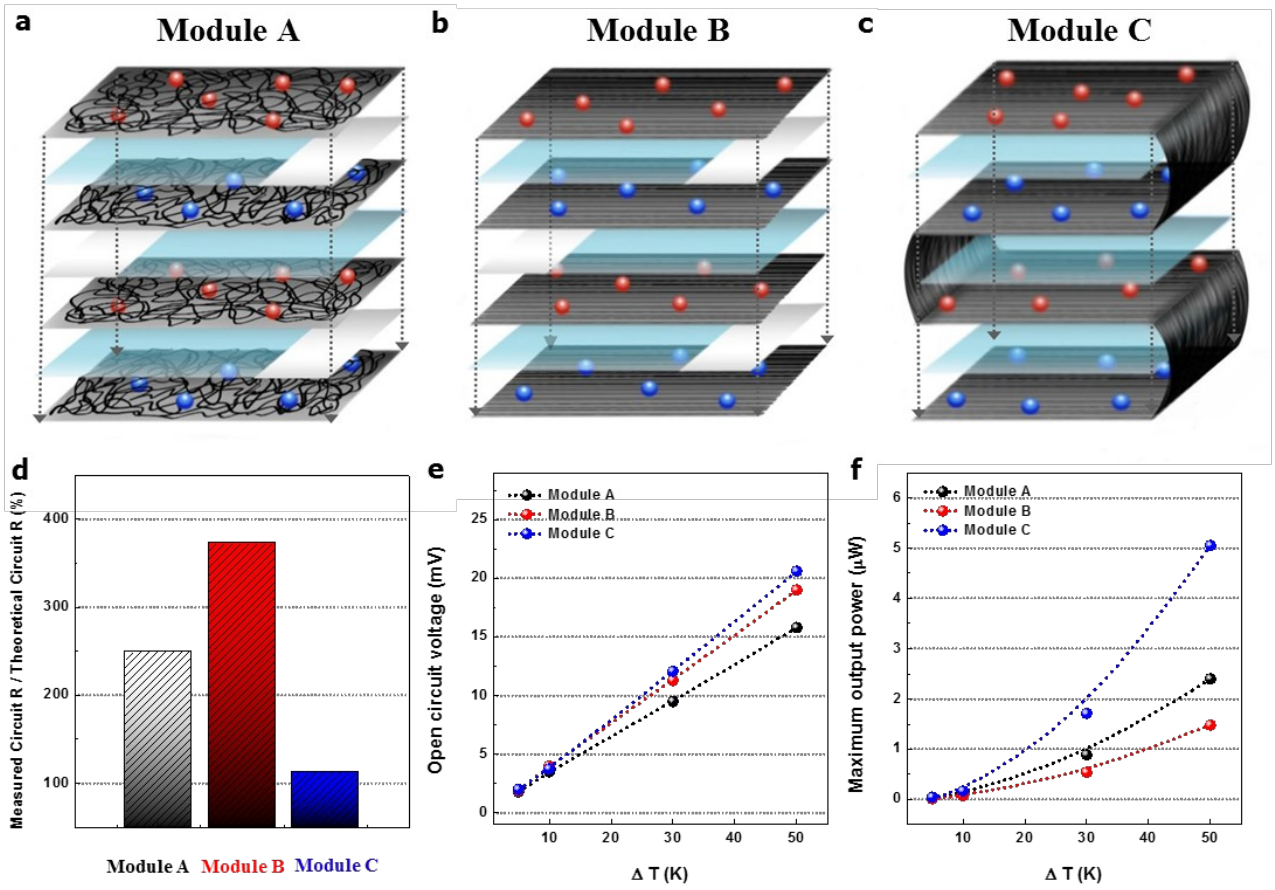

Figure 2. Schematic images of traditional stacked module based on (a) disordered SWCNT sheet, and (b) aligned CNT sheet interconnected by using Ag paste, (c) proposed continuous module based on aligned CNT sheet without additional metal electrodes. Light-blue and silver areas indicate the insulating layers and silver electrodes. Red and blue circles indicate *n*-type dopant (PEI) and *p*-type dopant ($FeCl_3$). Comparison of circuit resistance (d), open circuit voltage (e) and maximum output power (f) as a function of ΔT for the above three modules with 5 pairs of *p*- and *n*-doped CNT sheets.

Module B in 2b has the exact same design and fabrication method as Module A, but was prepared using the highly-aligned CNT sheets. Module C in 2c shows the continuous design based on the highly-aligned CNT sheets without metal electrodes as we proposed. Additional photographs of the prepared modules are provided in **Figure S5.** For the comparison study, the ratio of measured circuit resistance and theoretical circuit resistance for different modules is calculated, as shown in **Figure 2d**. The theoretical circuit resistance of the module was calculated by simply summing 10 of the single sheet resistances and neglects to take into account the impact of multiple contacts. Module A and Module B show 250% and 373% increased circuit resistance compared to their theoretical circuit resistance, alternatively, while module C shows a roughly equivalent circuit resistance compared with the theoretical calculation. According to this model, module B and module C should theoretically have the same resistance values because they are comprised of the same type of CNT sheet. However, there is a noticeable gap between the expected and measured circuit resistances for module B and module C, which is likely due to parasitic losses that arise when poor contact is made between the metal electrode and the CNT sheet. As is well known, the output power of TE module is mainly determined by both the TE properties of *p*- and *n*-type TE legs and the internal circuit resistance, especially at the interfaces, i.e. P = VI = V^2/¿¿, where V, I, and R are circuit voltage, current, and resistance, respectively. Theoretically, *P* has a

maximum value when internal and external resistances are exactly the same ($R_{int}=R_{ext}$).

As shown in **Figure 2e** and **2f**, although modules B and C (with/without metal electrodes) have similar open circuit voltage values, module C demonstrates enhanced power output due to it's minimized circuit resistance. When comparing modules A and C, module C exhibits a higher output power due to its higher open circuit voltage and lack of electrode interconnects. In summary, due to the intrinsically high *S* of aligned CNT sheet and the minimized circuit resistance, module C shows the highest output power among the three modules. The maximum output power of module C was 5.05 μW at ΔT=50 K when the external load resistance matches the internal resistance of the module, which shows a 210% and 355% enhancement compared to module A and module B, respectively. The output power results of modules A, B, and C at various ΔT were also provided in **Figure S6**. In all cases, we can achieve the same conclusion discussed above.

Fabrication of prototype *f*-TEG

In order to realize a freestanding *f*-TEG, we fabricated a flexible support with PDMS by using a home-made stainless steel mold in **Figure S7**. By adopting the continuous module design, the doped CNTs sheet was woven into the PDMS support unit to create a *f*-TEG device that is electrically in series and

thermally in parallel. Eventually, the doped CNT sheets face inside and are covered by the PDMS support unit. The undoped regions faced outside at the top and bottom side of the module, acting as electrodes. Detailed fabrication steps are explained in the experimental section. **Figure 3a** displays the schematic structure of the prototype *f*-TEG, with a typical module consisting of 9 p-n units shown in **Figure 3b**. The as-fabricated prototype *f*-TEG shows excellent flexibility and durability due to the continuous design fabricated with a single CNT sheet. This architecture is ideal for real-world implementation because when the *f*-TEG is exposed to strains or stress by being bent or pressured, there are no physical interconnects at risk of failing. To evaluate the power generation performance of the prototype *f*-TEG, a home-made measurement system (**Figure 3c)** was utilized. **Figure 3d** shows the performance of the prototype *f*-TEG to demonstrate the energy conversion potentials at different temperature conditions. As expected, the open circuit voltage of the device increased in proportion to the applied ΔT, achieving a maximum output voltage of 23 mV at a ΔT=50 K. The output power was also measured

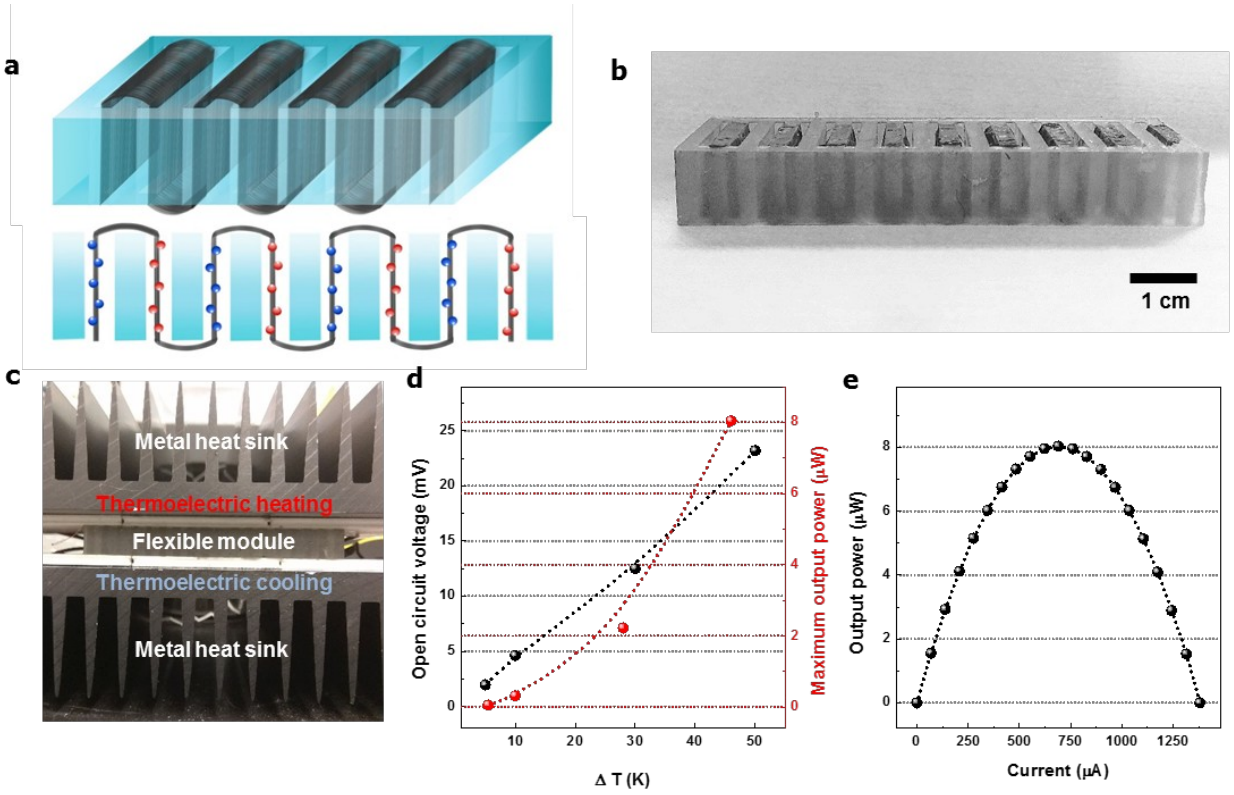

Figure 3. (a) The schematic structure of the prototype *f*-TEG. Light-blue areas indicate the PDMS supporting unit. Red and blue circles indicate n-type dopant (PEI) and p-type dopant ($FeCl_3$), respectively. (b) Photo image of the prototype *f*-TEG. (c) Photo image of the measurement system for TE power generation performance (d) Open circuit voltage and maximum power output of the prototype module as a function of ΔT. (e) Output power versus current curve of the prototype module at the 50 K of ΔT. Corresponding tests at different ΔT was given in SI.

at ΔT=50 K and is given in **Figure 3e**. We obtained 8 μW for the maximum output power with 17 Ω of the load resistance, which is superior compared to previous reports in CNT-based flexible TEGs.[1, 6, 35] We also provided additional output power results at various ΔT ranges (**Figure S8**). One of the

great advantages of our continuous module design is that it is possible to easily enhance the output power by both minimizing the circuit resistance and expanding the number of p-n pairs in series. With proper design and fabrication of the supporting unit, we can also increase the packing density of *f*-TEG and achieve higher power densities tailored to specific application needs.

Demonstration of wearable TEG

Finally, to demonstrate the bio-thermal harvest of electricity by body heat, we wore the prototype *f*-TEG as a wristband, as shown in **Figure 4a**. We achieved 3.4 mV of electrical potential directly converted from body heat without mechanical moving parts when the ΔT was ~7 K (as determined by the inserted IR thermal image). It is noteworthy that the generated voltage per unit weight of the prototype *f*-TEG is around 170 mV/g due to the lightweight nature of the CNT sheet, thereby only 9 g of CNT sheet is needed for generating the same potential of 1.5 V that a standard AA battery produces. These results show the great potential for powering personal wearable electronic devices. Moreover, in order to investigate the device reliability under mechanical stress, we measured the change of circuit resistance of the module under the bending status. As can be seen in **Figure 4b,** there's no significant increase (< 0.6%) of the circuit resistance, which implies high flexibility and electromechanical stability. Furthermore, the *f*-

TEG was repeatedly bent up 1000 cycles with a bending radius of 20 mm, which also exhibits a stable circuit resistance (< 2.3%). Therefore, the present *f*-TEG is mechanically robust, providing opportunities to reconfigure into various conformal structures, which would be a strong benefit for harvesting bio-thermal energy.

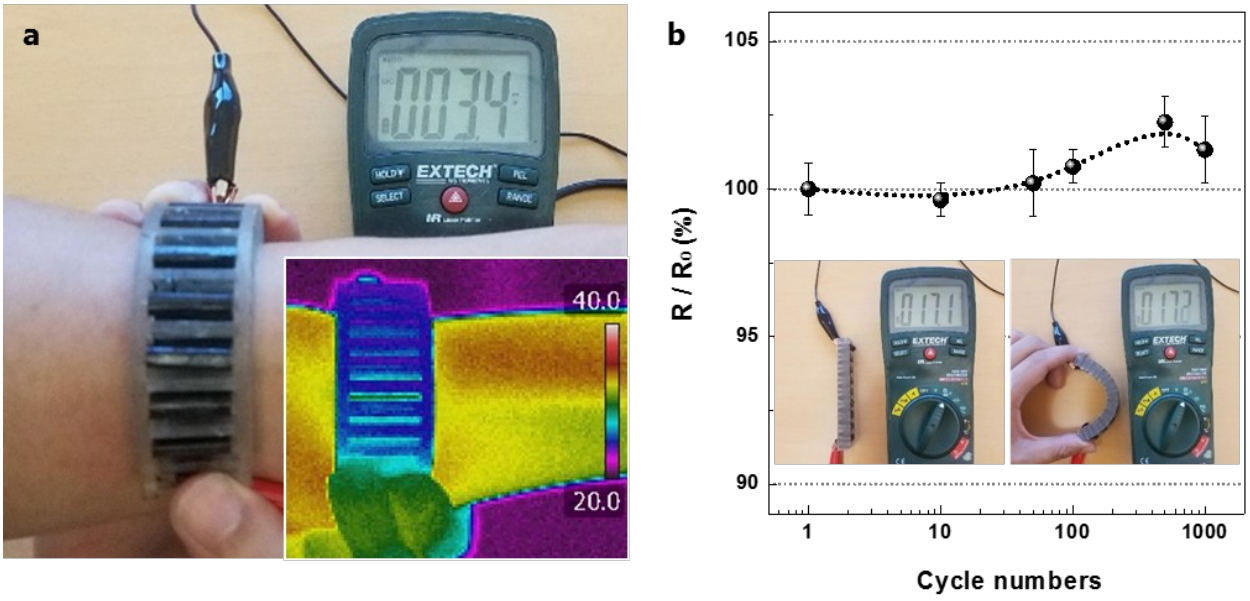

Figure 4. (a) Demonstration of bio-thermal energy harvesting from body heat. A thermal IR camera image is inserted. (b) Resistance changes as a function of bent cycles. The inserted images show the real measurement process.

Conclusion

In summary, in order to transfer the outstanding electrical and mechanical properties of CNTs into TE application, a light-weight, high performance, and robust *f*-TEG has been fabricated. The highly-aligned, free-standing CNT sheet imbues greatly improved electrical transport on both a microscale and macroscale basis. A single CNT sheet can be fabricated as both *p*, *n*-type TE legs and electrodes through facile solution doping processes, thus enabling the production of an entire *f*-TEG from a continuous sheet of material. The continuity of the material provides a significant reduction in contact resistance between TE legs and electrodes compared to traditional TEGs. This reduction in overall device resistance translates to a higher power output without a dramatic improvement in material performance. Based on this concept, the prototype *f*-TEG with 9 p-n pairs yields the maximum output power of 8 μW at a 50 K temperature gradient. In addition, its continuous module structure without any disconnected parts provides high degrees of mechanical stability and durability with little impact on device resistance. Moreover, this module actualizes the potential for *f*-TEGs to act as personal power devices harvesting energy from the human body. This ability stands poised to not only revolutionize the widespread deployment of TEGs as a whole, but also open new avenues for the development of a wide variety of cutting edge electronics such as biosensors, watches and other personal electronic devices that are hobbled by current power supply limitations.

Supporting Information

Raman spectra, TGA curve, XPS measurement, Thermoelectric properties measurement, Photo images of thermoelectric module, Thermoelectric power output curve, Photo images of stainless steel mold (PDF).

Corresponding Author

*E-mail: jjurban@lbl.gov

*E-mail: crpark@snu.ac.kr

*E-mail: heesukkim@kist.re.kr

Notes

The authors declare no competing financial interest.

Acknowledgment

This work was performed at the Molecular Foundry, Lawrence Berkeley National Laboratory, and was supported by the Department of Energy, Office of Science, Office of Basic Energy Sciences, Scientific User Facilities Division of the U.S. Department of Energy under Contract No. DE-AC02-05CH11231. This research was supported by Basic Science Research Program through the National Research Foundation of Korea (NRF) funded by the Ministry of Education (No. 2018R1A6A3A03012642) and also financially supported from

the R&D Convergence Program of NST (National Research Council of Science & Technology) (2N44620).

Reference

(1) Zaia, E. W.; Gordon, M. P.; Yuan, P.; Urban, J. J., Progress and Perspective: Soft Thermoelectric Materials for Wearable and Internet-of-Things Applications. *Adv. Electron. Mater.* **2019**, 1800823.

(2) Javey, A.; Guo, J.; Wang, Q.; Lundstrom, M.; Dai, H., Ballistic carbon nanotube field-effect transistors. *Nature* **2003,** *424*, 654-657.

(3) Iijima, S., Helical microtubules of graphitic carbon. *Nature* **1991,** *354*, 56.

(4) Cao, A.; Dickrell, P. L.; Sawyer, W. G.; Ghasemi-Nejhad, M. N.; Ajayan, P. M., Super-Compressible Foamlike Carbon Nanotube Films. *Science* **2005,** *310*, 1307-1310.

(5) Nonoguchi, Y.; Ohashi, K.; Kanazawa, R.; Ashiba, K.; Hata, K.; Nakagawa, T.; Adachi, C.; Tanase, T.; Kawai, T., Systematic Conversion of Single Walled Carbon Nanotubes into n-type Thermoelectric Materials by Molecular Dopants. *Sci. Rep.* **2013,** *3*, 3344.

(6) Blackburn, J. L.; Ferguson, A. J.; Cho, C.; Grunlan, J. C., Carbon-Nanotube-Based Thermoelectric Materials and Devices. *Adv. Mater.* **2018,** *30,* 1704386.

(7) Yu, C.; Choi, K.; Yin, L.; Grunlan, J. C., Light-Weight Flexible Carbon Nanotube Based Organic Composites with Large Thermoelectric Power Factors. *ACS Nano* **2011,** *5*, 7885-7892.

(8) Toshima, N.; Oshima, K.; Anno, H.; Nishinaka, T.; Ichikawa, S.; Iwata, A.; Shiraishi, Y., Novel Hybrid Organic Thermoelectric Materials:Three-Component Hybrid Films Consisting of a Nanoparticle Polymer Complex, Carbon Nanotubes, and Vinyl Polymer. *Adv. Mater.* **2015,** *27*, 2246-2251.

(9) Cho, C.; Wallace, K. L.; Tzeng, P.; Hsu, J.-H.; Yu, C.; Grunlan, J. C., Outstanding Low Temperature Thermoelectric Power Factor from Completely Organic Thin Films Enabled by Multidimensional Conjugated Nanomaterials. *Adv. Energy Mater.* **2016,** *6*, 1502168.

(10) Yu, C. H.; Ryu, Y.; Yin, L. A.; Yang, H., Modulating Electronic Transport Properties of Carbon Nanotubes To Improve the Thermoelectric Power Factor via Nanoparticle Decoration. *ACS Nano* **2011,** *5*, 1297-1303.

(11) Suemori, K.; Hoshino, S.; Kamata, T., Flexible and lightweight thermoelectric generators composed of carbon nanotube–polystyrene composites printed on film substrate. *Appl. Phys. Lett.* **2013,** *103*, 153902.

(12) Meng, C.; Liu, C.; Fan, S., A promising approach to enhanced thermoelectric properties using carbon nanotube networks. *Adv. Mater.* **2010,** *22*, 535-539.

(13) An, C. J.; Kang, Y. H.; Lee, A. Y.; Jang, K.-S.; Jeong, Y.; Cho, S. Y., Foldable Thermoelectric Materials: Improvement of the Thermoelectric Performance of Directly Spun CNT Webs by Individual Control of Electrical

and Thermal Conductivity. *ACS Appl. Mater. Interfaces* **2016,** *8*, 22142-22150.

(14) Hewitt, C. A.; Montgomery, D. S.; Barbalace, R. L.; Carlson, R. D.; Carroll, D. L., Improved thermoelectric power output from multilayered polyethylenimine doped carbon nanotube based organic composites. *J. Appl. Phys.* **2014,** *115*, 184502.

(15) Goldsmid, H. J., Bismuth Telluride and Its Alloys as Materials for Thermoelectric Generation. *Materials* **2014,** *7*, 2577-2592.

(16) Goldsmid, H. J., The Electrical Conductivity and Thermoelectric Power of Bismuth Telluride. *Proc. Phys. Soc.* **1958,** *71*, 633-646.

(17) He, W.; Zhang, G.; Zhang, X.; Ji, J.; Li, G.; Zhao, X., Recent development and application of thermoelectric generator and cooler. *Appl. Energy* **2015,** *143*, 1-25.

(18) Bahk, J.-H.; Fang, H.; Yazawa, K.; Shakouri, A., Flexible thermoelectric materials and device optimization for wearable energy harvesting. *J. Mater. Chem. C* **2015,** *3*, 10362-10374.

(19) Dresselhaus, M. S.; Dresselhaus, G.; Jorio, A., UNUSUAL PROPERTIES AND STRUCTURE OF CARBON NANOTUBES. *Annu. Rev. Mater. Res.* **2004,** *34*, 247-278.

(20) Avery, A. D.; Zhou, B. H.; Lee, J.; Lee, E. S.; Miller, E. M.; Ihly, R.; Wesenberg, D.; Mistry, K. S.; Guillot, S. L.; Zink, B. L.; Kim, Y. H.; Blackburn, J. L.; Ferguson, A. J., Tailored semiconducting carbon nanotube networks with enhanced thermoelectric properties. *Nat. Energy* **2016,** *1*, 16033.

(21) Zheng, M.; Jagota, A.; Semke, E. D.; Diner, B. A.; McLean, R. S.; Lustig, S. R.; Richardson, R. E.; Tassi, N. G., DNA-assisted dispersion and separation of carbon nanotubes. *Nat. Mater.* **2003,** *2*, 338-342.

(22) Arnold, M. S.; Green, A. A.; Hulvat, J. F.; Stupp, S. I.; Hersam, M. C., Sorting carbon nanotubes by electronic structure using density differentiation. *Nat. Nanotechnol.* **2006,** *1*, 60-65.

(23) Lim, s. c.; Jang, J.; Bae, D.; Han, G.; Lee, S.; Yeo, I.-S.; Lee, Y., Contact resistance between metal and carbon nanotube interconnects: Effect of work function and wettability. *Appl. Phys. Lett.* **2009,** *95*, 264103-264103.

(24) Dag, S.; Gülseren, O.; Ciraci, S.; Yildirim, T., Electronic structure of the contact between carbon nanotube and metal electrodes. *Appl. Phys. Lett.* **2003,** *83*, 3180-3182.

(25) Lee, J.-O.; Park, C.; Kim, J.-J.; Kim, J.; Park, J. W.; Yoo, K.-H., Formation of low-resistance ohmic contacts between carbon nanotube and metal electrodes by a rapid thermal annealing method. *J. Phys. D: Appl. Phys.* **2000,** *33*, 1953-1956.

(26) Choi, J.; Jung, Y.; Yang, S. J.; Oh, J. Y.; Oh, J.; Jo, K.; Son, J. G.; Moon, S. E.; Park, C. R.; Kim, H., Flexible and Robust Thermoelectric Generators Based on All-Carbon Nanotube Yarn without Metal Electrodes. *ACS Nano* **2017,** *11*, 7608-7614.

(27) Baughman, R. H.; Zakhidov, A. A.; de Heer, W. A., Carbon nanotubes--the route toward applications. *Science* **2002,** *297*, 787-792.

(28) Jorio, A.; Dresselhaus, G.; Dresselhaus, M. S.; Souza, M.; Dantas, M. S. S.; Pimenta, M. A.; Rao, A. M.; Saito, R.; Liu, C.; Cheng, H. M., Polarized Raman Study of Single-Wall Semiconducting Carbon Nanotubes. *Phy. Rev. Lett.* **2000,** *85*, 2617-2620.

(29) Snyder, G. J.; Toberer, E. S., Complex thermoelectric materials. *Nat. Mater.* **2008,** *7*, 105-114.

(30) Hayashi, D.; Ueda, T.; Nakai, Y.; Kyakuno, H.; Miyata, Y.; Yamamoto, T.; Saito, T.; Hata, K.; Maniwa, Y., Thermoelectric properties of single-wall carbon nanotube films: effects of diameter and wet environment. *Appl. Phys. Express* **2016,** *9*, 025102.

(31) Ryu, Y.; Freeman, D.; Yu, C., High electrical conductivity and n-type thermopower from double-/single-wall carbon nanotubes by manipulating charge interactions between nanotubes and organic/inorganic nanomaterials. *Carbon* **2011,** *49*, 4745-4751.

(32) Shim, M.; Javey, A.; Shi Kam, N. W.; Dai, H., Polymer functionalization for air-stable n-type carbon nanotube field-effect transistors. *J. Am. Chem. Soc.* **2001,** *123*, 11512-11513.

(33) Duong, D. L.; Lee, I. H.; Kim, K. K.; Kong, J.; Lee, S. M.; Lee, Y. H., Carbon nanotube doping mechanism in a salt solution and hygroscopic effect: density functional theory. *ACS Nano* **2010,** *4*, 5430-5436.

(34) Kim, S. M.; Kim, K. K.; Jo, Y. W.; Park, M. H.; Chae, S. J.; Duong, D. L.; Yang, C. W.; Kong, J.; Lee, Y. H., Role of anions in the $AuCl_3$-doping of carbon nanotubes. *ACS Nano* **2011,** *5*, 1236-1242.

(35) Hewitt, C. A.; Kaiser, A. B.; Roth, S.; Craps, M.; Czerw, R.; Carroll, D. L., Multilayered Carbon Nanotube/Polymer Composite Based Thermoelectric Fabrics. *Nano Lett*. **2012**, *12*, 1307-1310.

TOC

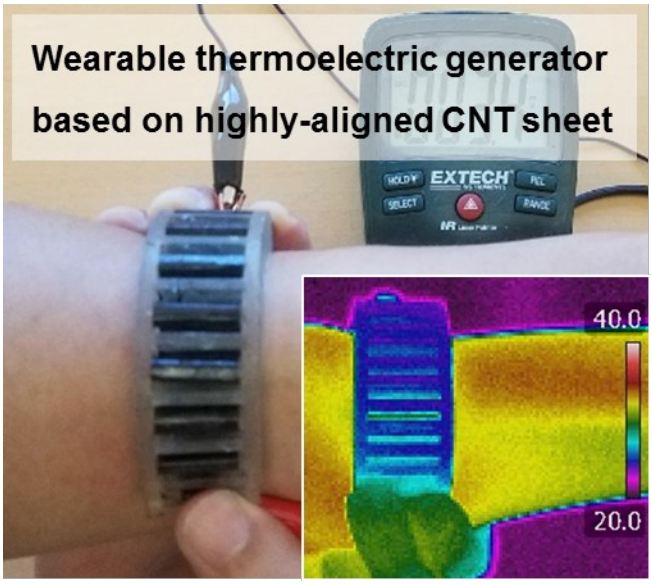
Wearable thermoelectric generator
based on highly-aligned CNT sheet
EXTECH
40.0
20.0